

# Bounds on Compactness for LMXB Neutron Stars from X-ray Burst Oscillations

Nitya R. Nath<sup>1,2</sup>, Tod E. Strohmayer & Jean H. Swank

*Laboratory for High Energy Astrophysics, NASA's Goddard Space Flight Center, Greenbelt,  
MD 20771; stroh@clarence.gsfc.nasa.gov*

`stroh@clarence.gsfc.nasa.gov`

## ABSTRACT

We have modelled X-ray burst oscillations observed with the Rossi X-ray Timing Explorer (RXTE) from two low mass X-ray binaries (LMXB): 4U 1636-53 with a frequency of 580 Hz, and 4U 1728-34 at a frequency of 363 Hz. We have computed least squares fits to the oscillations observed during the rising phase of bursts using a model which includes emission from either a single circular hot spot or a pair of circular antipodal hot spots on the surface of a neutron star. We model the spreading of the thermonuclear hot spots by assuming that the hot spot angular size grows linearly with time. We calculate the flux as a function of rotational phase from the hot spots and take into account photon deflection in the relativistic gravitational field of the neutron star assuming the exterior space-time is the Schwarzschild metric. We find acceptable fits with our model in a  $\chi^2$  sense, and we use these to place constraints on the compactness of the neutron stars in these sources. For 4U 1636-53, in which detection of a

---

<sup>1</sup>Raytheon ITSS, Lanham, MD 20706

<sup>2</sup>Currently with: Science Systems and Applications, Lanham, MD 20706

290 Hz sub-harmonic supports the two spot model, we find that the compactness (i.e., mass/radius ratio) is constrained to be  $M/R < 0.163$  at 90 % confidence ( $G = c = 1$ ). This requires a relatively stiff equation of state (EOS) for the stellar interior. For example, if the neutron star has a mass of  $1.4M_{\odot}$  then its radius must be  $> 12.8$  km. Fits using a single hot spot model are not as highly constraining. We discuss the implications of our findings for recent efforts to calculate the EOS of dense nucleon matter and the structure of neutron stars.

*Subject headings:* structure of stars - equations of state - stars: individual (4U 1636-53, 4U 1728-34) - stars: neutron - stars: oscillations - X-rays: bursts

## 1. Introduction

X-ray brightness oscillations with frequencies in the 300 - 600 Hz range have now been observed during thermonuclear X-ray bursts from 10 LMXB systems (see Strohmayer 2001 for a recent review). Substantial evidence suggests that rotational modulation of a localized hot spot or a pair of antipodal spots is responsible for the observed oscillations, especially during the rising phase (see for example Strohmayer, Zhang & Swank 1997; Heise 2000). As the mass to radius ratio,  $M/R$  or “compactness”, of a neutron star increases, the deflection of photons by its relativistic gravitational field becomes stronger and consequently a greater fraction of the stellar surface is visible to an observer at any given time. This effect weakens the spin modulation pulsations produced by a rotating hot spot on the neutron star surface. Because of this effect, Strohmayer et al. (1997) suggested that modelling of the burst oscillation amplitude could in principle provide a constraint on the neutron star compactness. Strohmayer, Zhang & Swank (1997) investigated the temporal evolution of the amplitude of burst oscillations from 4U 1728-34 and showed that a simple model of an expanding hot spot on a neutron star was in qualitative agreement with the data. Miller &

Lamb (1998) performed a study of the dependence of the oscillation amplitude from a point-like hot spot on the stellar compactness, the surface rotational velocity, and the spectrum of the surface emission, and showed that if two antipodal spots are present, the resulting limits on the compactness can be highly constraining. Weinberg, Miller, & Lamb (2000) have recently performed similar calculations but allow for hot spots of finite size. Psaltis, Ozel, & DeDeo (2001) have also recently investigated the effects of relativistic photon deflection on the inferred properties of thermally emitting neutron stars.

Miller (1999) reported the detection of a 290 Hz sub-harmonic of the stronger 580 Hz oscillation frequency in a study of 5 bursts from 4U 1636-53. This led him to suggest that the neutron star spin frequency is actually 290 Hz in this source and that two antipodal hot spots produce the 580 Hz modulation. The observation of a pair of high frequency quasi-periodic oscillations (QPO) with a frequency separation of  $\sim 251$  Hz in this source (Mendez, van der Klis, & van Paradijs 1998), has also been interpreted, in the context of a beat frequency model for the high frequency QPO, as evidence for a neutron star spin frequency of  $\sim 290$  Hz rather than 580 Hz (see Miller, Lamb & Psaltis 1998). We note, however, that recent efforts to confirm the sub-harmonic detection in subsequent bursts from 4U 1636-53 have not been successful (Strohmayer 2001).

Strohmayer et al. (1998a) reported very large amplitude oscillations at 580 Hz during the rising phase of some bursts from 4U 1636-53. This combination of large measured amplitudes near burst onset and the evidence that two hot spots may produce the modulation, make 4U 1636-53 perhaps the best source currently known in which to constrain the neutron star mass and radius based on the properties of burst oscillations. Here we report on our efforts to do this by detailed modelling of the burst oscillations observed during the rising phase of bursts. We focus on 4U 1636-53 because if the two hot spot conjecture is correct for this object then our results place strong constraints on the neutron star compactness. However, we also

summarize our results for 4U 1728-34, a source which has also shown strong oscillations during the rising phase of bursts. The plan of this paper is as follows. In §2 we discuss the basic features and assumptions of our model. In §3 we outline the method of calculation. In §4 we describe our model fitting procedures and our results for both single and antipodal hot spot models. We also summarize the results of fits to data from 4U 1636-53 and 4U 1728-34. In §5 we summarize our results and discuss them in the context of recent efforts to constrain the EOS of neutron star matter. We also discuss future steps we will take to improve the hot spot model.

## 2. Model Assumptions

Both spectral and temporal evidence indicate that the X-ray emission near the onset of at least some thermonuclear bursts is localized to a “hot spot” which spreads in some fashion until eventually encompassing all of the neutron star surface (see for example Strohmayer, Zhang & Swank 1997). This likelihood was also recognized early on in theoretical studies of thermonuclear bursts (Joss 1978). Motivated by this we model the burst rise by assuming that all the burst emission comes from either one or a pair of circular hot spots which expand linearly in angular size with time. The rest of the neutron star surface is assumed dark. Photon trajectories are computed assuming the Schwarzschild metric describes the space-time exterior to the star. This is a reasonable approximation since the influence of the neutron star’s rotation on the space-time only affects the oscillation amplitude to second order (Miller & Lamb 1996). For the present work we shall only investigate bolometric modulations across the full  $\sim 2 - 90$  keV bandpass of the RXTE Proportional Counter Array (PCA). We shall also ignore Doppler shifts and relativistic aberration produced by the rotational motion of the hot spot (see for example Miller 1999; Chen & Shaham 1989). We discuss later the likely influence on our results of this approximation.

Our model is uniquely characterized by seven parameters: (1) an overall source intensity or normalization,  $S$ , which can be thought of as the flux leaving unit surface area of the neutron star. (2) neutron star compactness,  $\beta = M/R$ , where  $M$  and  $R$  are the stellar mass and radius, respectively, (3) initial angular size of the spot (half of the subtended angle),  $\alpha_0$ , (4) angular growth rate of the hot spot,  $\dot{\alpha}$ , (5) initial rotational phase,  $\delta_0$ , (6) latitude of the spot center,  $\theta_s$ , measured from the rotational equator, and (7) latitude of the observers line of sight,  $\theta_{obs}$ , also measured from the rotational equator. One of our primary goals is to determine an upper bound on the compactness. To do this within the context of our model we set the hot spot latitude and observation latitude to zero. That is, both the hot spots and the line of sight to the observer are centered on the rotational equator. This geometry produces the largest possible modulation amplitude. Since any observed modulation must be equal to or less than this limit, and since the modulation amplitude decreases with increasing compactness, the upper limit follows. For completeness, we also investigate the influence of moving the hot spot and the line of sight off the rotational equator. The geometry of our model is illustrated in Figure 1. Related hot spot models have been worked out by Pechenick, Ftaclas, & Cohen (1983) and Strohmayer (1992).

### 3. Method of Calculation

The geometry of a photon trajectory in relation to the observers line of sight  $\vec{r}_{obs}$  is shown in Figure 1. The figure is drawn with  $\theta_s = \theta_{obs} = 0$ . For any single point on the hot spot with radius vector  $\vec{r}$ , the path of a photon reaching the observer lies in the plane of  $\vec{r}$  and  $\vec{r}_{obs}$ , and is asymptotically parallel to  $\vec{r}_{obs}$  with impact parameter  $b$ . The two angles,  $\phi$  (between  $\vec{r}$  and  $\vec{r}_{obs}$ ) and  $\psi$  (the emission angle with respect to the surface normal), complete the description. For non-zero  $\theta_s$  and  $\theta_{obs}$ , the deflection geometry remains the same, only the plane in which the desired trajectory lies (the plane of  $\vec{r}$  and  $\vec{r}_{obs}$ ) changes. The angle  $\phi$

can be expressed as,

$$\phi = \int_0^{\sin^{-1}(\hat{b})} \left[ 1 - 2(M/R)(1 - \sin^3 y/\hat{b})/(1 - \sin^2 y) \right]^{-1/2} dy, \quad (1)$$

where  $\hat{b} = b/b_{max}$  is the reduced impact parameter,  $b_{max} = R(1 - 2(M/R))^{-1/2}$ , and  $M$  and  $R$  are the stellar mass and radius respectively. This form for the angle  $\phi$  is somewhat non-standard compared to previous work. More commonly  $\phi$  is expressed as

$$\phi = \int_0^{M/R} [u_b^2 - (1 - 2u)u^2]^{-1/2} du, \quad (2)$$

where  $u_b \equiv M/b$  (see for example, Pechenick, Ftaclas & Cohen 1983; Miller & Lamb 1998). Our rationale for rewriting the integrand is twofold; first, to explicitly show what parameters  $\phi$  depends on, and second to remove singular behavior of the integrand to facilitate numerical evaluation of the integral. Changing variables in (2) to  $u = (M/R)x$  results in the following expression;

$$\phi = \int_0^1 \left[ \hat{b}^{-2} \left( 1 - \frac{2M}{R} \right) - \left( 1 - \frac{2M}{R}x \right) x^2 \right]^{-1/2} dx. \quad (3)$$

As  $M/R$  becomes small this integral has the form,

$$\phi = \int_0^1 [\hat{b}^{-2} - x^2]^{-1/2} dx, \quad (4)$$

which has singular behavior as  $\hat{b}$  and  $x$  approach unity. The second change of variables to  $y = \sin^{-1} \hat{b}x$  is motivated by the form of equation (4) above, whose solution corresponds to the inverse sine function. With this final substitution we arrive at the expression in equation (1), which explicitly shows the dependence of  $\phi$  on  $M/R$  and  $\hat{b}$ , and is well defined and non singular. As  $\hat{b}$  varies from 0 to 1,  $\phi$  varies from 0 to  $\phi_{max}$ , the maximum value of  $\phi$ , which is attained when a photon is emitted tangentially to the stellar surface. We note several interesting limiting cases; for  $M/R = 0, 0.284, 0.331, 0.33333$ , we have  $\phi_{max} = \pi/2, \pi, 2\pi$ , and  $\infty$ , respectively. The last case,  $\phi_{max} = \infty$ , corresponds to the bound photon orbit at  $M/R = 1/3$ .

To compute the flux as a function of rotational phase we first invert  $\phi$  ( $\hat{b}, M/R$ ) numerically to obtain tables of  $\hat{b}$  as a function of  $\phi$  and  $M/R$ . We use Gaussian quadratures to solve the integral numerically. The method is fast and converges quickly. For a given  $M/R$  and each  $\phi = \cos^{-1}(\vec{r} \cdot \vec{r}_{obs})$  we then find  $\hat{b}$  and compute  $\cos \psi = (1 - \hat{b}^2)^{1/2}$ . The observed flux is then given by  $\int I_\nu \cos \psi d\Omega$ , where  $I_\nu$  is the local specific intensity at the surface of the neutron star, and the integral is carried out over the hot spot or spots. For the specific intensity we use both an isotropic emission function,  $I_\nu = 1$  and an angular dependent beaming function consistent with emission from a grey scattering atmosphere,  $I_\nu = 3/5 \cos \psi + 2/5$  (see Chandrasekhar 1960). Such a function should be appropriate for bursting neutron star atmospheres which are dominated by Thomson scattering (London, Taam, & Howard 1986). Figure 2 shows several examples of light-curves computed with our model using one hot spot and different values of  $M/R$ . The decrease in modulation amplitude with increasing compactness is clearly evident.

#### 4. Data Analysis Procedures and Results

We searched the available RXTE data from 4U 1636-53 and 4U 1728-34 for bursts and selected for analysis four from 4U 1636-53 and two from 4U 1728-34 which showed particularly strong oscillations during the rising phase. The data are in the form of X-ray event times recorded with  $125 \mu\text{s}$  resolution across the full 2 - 90 keV PCA bandpass. In order to fit our model we first break up the rising interval from each burst into a number,  $n_{interval}$ , of contiguous subintervals. Within each subinterval we epoch fold the data into  $n_{bin}$  phase bins using the oscillation frequency determined from a power spectral analysis of the entire rising interval. We then perform a  $\chi^2$  minimization by computing  $\chi^2 = \sum_{i=1}^N (O_i - M_i)^2 / \sigma^2$ . Here  $O_i$  and  $M_i$  are the numbers of observed and predicted counts, respectively, in the  $i^{\text{th}}$  data bin. For  $\sigma^2$  we use the Poisson variance, which is simply equal to the number of counts

in the bin. In general we also add a constant background level to the model as a way of modeling the pre-burst, accretion driven flux, which we assume is not associated with the burst. This also implies a tacit assumption that the accretion driven flux is not significantly altered by the burst. This quantity is well determined by the pre-burst data, so typically we do not treat it as a model parameter. In general the total length of data that we fit does not extend all the way to the peak of the burst for a number of reasons. The oscillation has usually dropped below our detection threshold before the peak is reached and often episodes of radius expansion also begin before the count rate reaches a maximum. In general, our assumptions regarding the growth of the hot spot should be most valid the closer we remain to the onset of the burst. This also tends to maximize our signal to noise ratio in data from a given burst since the modulation amplitude is largest near burst onset.

We minimize  $\chi^2$  using the Marquardt-Levenberg method and we can simultaneously vary all seven model parameters. Our choice regarding the number of data bins is a tradeoff between having sufficient counts in each bin and the need to have enough time resolution to adequately model the rise of the burst and hence constrain the hot spot spreading speed,  $\dot{\alpha}$ . In general we found that  $n_{region} = 8$  and  $n_{bin} = 8$  gave the best results. With this choice we have a total of 64 data bins. We also restrict  $M/R \leq 0.284$ , the limit beyond which photons from a given point on the stellar surface can reach the observer along more than one unique path. In general we find acceptable fits using both one and two hot spots for both sources. In the remainder we will summarize our results and discuss the implications for neutron star compactness, concentrating on the two spot fits for 4U 1636-53 for the reasons outlined above.

#### 4.1. Antipodal Hot Spot Models

Our best fitting models for bursts from 4U 1636-53 using two antipodal hot spots and the grey atmosphere intensity function are summarized in Table 1, where for each burst we give the observation date, the length of the time interval in which we fit the data, the best fitting model parameters and the minimum  $\chi^2$ . For these fits we have fixed to zero both the spot latitude,  $\theta_s$  and the observers latitude,  $\theta_{obs}$ , and we used 64 data bins. With 5 free parameters we therefore have 59 degrees of freedom. Our minimum  $\chi^2$  values are all statistically acceptable, indicating that the simple rotating hot spot model is consistent with the data. In Figure 3 we show the two spot fits for each of the four bursts from 4U 1636-53. Each panel shows the count rate in the PCA for the rising interval of a burst. The bursts are labelled by date. The vertical dashed lines denote the region in which we fit our model. The solid curve shows the best fitting model *extrapolated* to the time at which the entire surface of the neutron star is covered by the hot spots. The time resolution in these plots is not sufficient to resolve the oscillations, rather, this figure is meant to give the reader an assessment of how well the model does in describing the gross time evolution of each burst. There are several things to note from Figure 3. First, the fits *within* each interval are quite good, and they also extrapolate beyond the fitting interval rather well over a limited portion of the burst rise. The deviations at later times are not unexpected since in several of these bursts episodes of photospheric radius expansion begin at about the same time as the model begins to deviate from the burst rise. Indeed the burst on 08/20/98 did not show radius expansion and in this case the model extrapolates rather well for most of the rise. All the other bursts show radius expansion near the time that the model deviates from the data. Second, the maximum count rates inferred from our model for bursts 12/28/96 and 08/19/98 are quite similar. Since these bursts were quite similar in their peak fluxes, the model normalizations, which can be thought of as an averaged description of the thermonuclear burning, should also be similar and indeed they are. Note that though these two bursts have similar peak fluxes

they do not have similar rise times, and our model successfully accounts for this difference. Although the models are clearly inadequate to describe the details of the *entire* burst rise, they do better the closer one stays to the burst onset, and this behavior is the most relevant with regard to fitting the oscillations and constraining  $M/R$ .

Figure 4 graphically illustrates how well the model can fit the observed oscillations by comparing the best fit model and data for several different fits to the 12/28/96 burst from 4U 1636-53. Shown are the best fitting two spot model with  $\theta_s = \theta_{obs} = 0$  (solid); the best fitting one spot model with  $\theta_s = \theta_{obs} = 0$  (dashed); and the best fitting one spot model with all parameters free to vary (dotted). Since fits to the other bursts all look very similar we did not feel it was essential to show similar plots for each individual burst.

The derived best-fit compactness for the four bursts from 4U 1636-53 span a rather tight range from  $\beta = 0.075$  to  $0.134$ . In Figure 5 we show the best-fit values of  $M/R$  and their uncertainties. We fit a constant,  $\beta_{avg}$ , to the four values and find they are consistent with a single value for the compactness of  $\beta_{avg} = 0.126$  (solid horizontal line in Figure 5). The  $\chi^2$  per degree of freedom for the fit was 0.2. In order to derive a firm upper limit on the compactness we investigated the confidence region for  $\beta_{avg}$  and found the values of  $\beta$  which increased  $\chi^2$  by 2.71 (for 90% confidence) and 6.63 (for 99% confidence). These values are also shown in Figure 5 as the dashed (90%) and dot-dashed (99%) horizontal lines in Figure 5. The derived upper limits are  $\beta_{90\%} = 0.163$  and  $\beta_{99\%} = 0.183$ .

Since we do not in general know the orientation of the binary systems in which the neutron stars reside we performed the fitting under the assumption that the hot spot and observer are both in the plane of the rotational equator. This geometry gives the maximum rotational modulation. Thus each fitted value for  $\beta$  from a different burst gives a measure of the maximum allowable compactness of the neutron star. However, each individual measurement has associated with it a rather large uncertainty. Thus, our methodology in deriving

an upper limit on  $\beta$  is to combine a number of these independent measurements in order to reduce the overall uncertainty. In this way  $\beta_{avg}$  is our best estimate of how large the compactness of the neutron star is, but this estimate too is not exact and has a confidence region associated with it. It is the confidence region on  $\beta_{avg}$  that we use to determine a final upper limit. This may not be a unique statistical methodology, but we feel it is reasonable given the nature of the other model assumptions we have made. We will discuss the implications of our compactness limits for the neutron star EOS in the next section.

We also computed fits allowing the two angles  $\theta_s$  and  $\theta_{obs}$  to vary. As might be expected we find the inclusion of the additional parameters improves the fits, but only marginally. With these parameters free to vary we find that  $M/R$  tends to decrease, and both  $\theta_s$  and  $\theta_{obs}$  move off the rotational equator. We find, however, no stationary solutions in  $M/R$  with all seven parameters varying. These results serve to illustrate the basic correlation between compactness and the hot spot and viewing geometries. If the spot moves or is viewed away from the rotational equator then the inferred value of  $M/R$  must decrease in order to make up for the loss of modulation amplitude produced by a less than favorable geometry. Since realistic neutron star EOSs cannot support stars with arbitrarily small  $M/R$ , if the two spot model is correct, then our results suggest that the hot spots must be relatively near the rotational equator in order to achieve the high observed amplitudes. If the hot spots are linked to the poles of a magnetic field in 4U 1636-53 (see Miller 1999), then this would suggest that the magnetic axis would have to be nearly perpendicular to the rotation axis. If we assume the surface emission is isotropic, the fits for all the bursts are very similar, but the  $M/R$  values are systematically lower, with the weighted mean dropping to  $M/R = 0.05$ . This is as expected, since isotropic emission produces a lower amplitude than the grey atmosphere beaming function.

Our results for 4U 1728-34 are quite similar to those derived for 4U 1636-53. The results

of the two spot fits for bursts from 4U 1728-34, with  $\theta_s$  and  $\theta_{obs}$  fixed at zero and with beamed emission are also shown in Table 1. The weighted average of the two fits yields the value  $M/R = 0.121$ , with 90% and 99% confidence upper limits of 0.171 and 0.199, respectively. These are similar to the limits derived for 4U 1636-53. Although no sub-harmonic has been detected for this source, the closeness of the derived  $M/R$  limits for the two sources is striking, and may be an indication that, irrespective of the model, the actual compactness of the two sources is similar.

#### 4.2. One Spot Models

For one spot models we generally find there are no strong constraints on the compactness for either source. This results from the fact that stars even as compact as our computational limit,  $M/R = 0.284$ , can still produce a sufficiently large modulation amplitude to match the data. For example, the best fits for the 4U 1636-53 bursts with four parameters varying (ie.,  $M/R$  fixed at 0.284,  $\theta_s$  and  $\theta_{obs}$  fixed at zero), and with beamed emission, give  $\chi^2 = 69.4$ , 66.2, 70.6, and 75.0, for each burst respectively. These values are marginally higher than for the corresponding two spot fits, however, from a statistical point of view they are still formally acceptable. For the one spot fits we find that  $\chi^2$  monotonically decreases as  $M/R$  increases from 0 to 0.284, but never reaches a minimum. In other words we find no meaningful upper limit to the compactness, at least within the confines of our model assumptions. A comparison of the  $\chi^2$  values between the two spot and one spot fits at first glance seems to suggest that the two spot fits are better, however, this is misleading because the one spot fits are not stationary in  $M/R$ , that is they have not converged to a minimum.

## 5. Discussion and Summary

We have shown that if two hot spots produce the observed modulation at 580 Hz in 4U 1636-53 then the large amplitude of oscillations near burst onset provide a strong constraint on the compactness. In Figure 6 we show in the mass - radius plane our 90 and 99 % confidence upper limits on the compactness  $\beta = M/R$  for 4U 1636-53 from our two hot spot fits. The shaded region denotes the ranges of  $M$  and  $R$  which satisfy our compactness constraint and have  $M > 1.4M_{\odot}$ , which we take as a reasonable estimate of the minimum mass of the neutron star in these old accreting systems. We also show several theoretical neutron star EOSs which span a range of stiffnesses based on current uncertainties in the exact composition of neutron star matter and our incomplete knowledge of the nucleon - nucleon interaction. Also shown in Figure 6 is our computational limit at  $M/R \leq 0.284$  (solid diagonal line).

As can be seen our results tend to favor moderately stiff to very stiff EOSs. For example, our limits are comfortably consistent with EOS L (Pandharipande & Smith 1975). However, the most recent theoretical calculations of neutron star EOSs which are consistent with the currently available nucleon scattering data are generally not as stiff as this EOS (see for example Akmal, Pandharipande & Ravenhall 1998). For example, the best EOS of Akmal, Pandharipande & Ravenhall (1998), which is denoted APR in Figure 6, is barely consistent with our 99% limit. However, these modern EOSs are still not rigorously self consistent, and become “superluminal” (the sound speed exceeds the speed of light) above some density. Modifications to the EOS can be made in an ad hoc manner by setting the sound speed equal to the speed of light above some critical or “matching” density (see for example Heiselberg & Hjorth-Jensen 1999) . This has the effect of stiffening the EOS. Recently, Olson (2001) has investigated changes to the high density EOS of neutron star matter required by constraints derived from relativistic kinetic theory. In Figure 6 we show two of these modifications to

the APR EOS. The thick dashed lines show the APR EOS modified by the kinetic theory constraints for two different matching densities,  $0.316 \text{ fm}^{-3}$  (APR-Kin1) and  $0.270 \text{ fm}^{-3}$  (APR-Kin2) (see Olson 2001 for a detailed discussion). With the kinetic theory assumptions the APR EOS is now reasonably consistent with our limits.

Recently, Lattimer & Prakash (2000) have argued that measurements of the neutron star radius to about 10% precision should be sufficient to usefully constrain the neutron star EOS. They showed that as long as extreme softening of the EOS does not occur in the vicinity of nuclear matter equilibrium density then the stellar radius is almost independent of the mass. Since observed neutron star masses cluster rather closely around  $1.4 M_{\odot}$  they argued that the more important quantity in terms of constraining the EOS is the stellar radius. Since the neutron stars in LMXBs are upwards of  $10^8$  yr old and they have been accreting most of their lifetime, it is very likely that they are at least more massive than the  $1.4 M_{\odot}$  typically found for younger neutron stars (Thorsett & Chakrabarty 1999). If this is the case, then our results place a rather firm lower limit on  $R$  of about 11.5 km. Such a limit is consistent with the notion that extreme softening of the EOS, as can be produced by pion, kaon or other hyperon condensates, does not occur in neutron star cores (see Lattimer & Prakash 2000). Since these inferences depend crucially on the two hot spot hypothesis for the burst oscillations from 4U 1636-53, it is vital to try and settle this issue in the near future.

We have generally tried to employ the simplest assumptions consistent with maintaining the essential physics of the model and the observed properties of the bursts. For this work we have neglected the Doppler shifts and relativistic aberration produced by the rapid motion of the hot spots. Although we do not know the rotational velocity precisely because of our uncertainty in the stellar radius and the number of hot spots, it is likely that the velocity on the rotational equator is  $\leq 0.1 c$ . Miller & Lamb (1998) investigated the effects of the

rotational velocity of a point spot on the bolometric and energy dependent amplitude and showed that although such a velocity can have important effects on the amplitude measured at particular photon energies, they also showed that the effect on the bolometric amplitude of the rotational velocity is very modest (see their Figure 1d; see also Weinberg, Miller & Lamb 2000). The calculations of Miller & Lamb (1998) were for point-like spots and hence represent upper limits to the size of any rotational effect. Since our model uses spots of a finite and growing angular size, the rotational effects, which represent an integral of the line of sight rotational velocity over the hot spot, must be less than the estimates computed by Miller & Lamb (1998). The amplitude of higher harmonics is more sensitive to the rotational velocity; however, the present RXTE data are not very sensitive to the shape of the pulses, i.e., we do not detect any higher harmonics, nor do we know of any published reports of significant harmonics of burst oscillations. Based on this and because we only investigate the bolometric amplitude we believe we are justified in neglecting the Doppler effects for the present work. However, by not investigating the energy dependent effects we are indeed ignoring some useful information which can eventually help provide more powerful constraints on  $M$  and  $R$ . We plan to improve our model by including these energy dependent effects and will report the results from such a study in a sequel.

Using our model we have also begun to investigate the constraints that can be obtained with data of a higher statistical precision than presently available. We have found that the present RXTE data is essentially insufficient for constraining the hot spot and viewing geometry. However, if the count rate were increased by a factor of 10 - 20 times the RXTE rate then our simulations suggest that it will be possible to simultaneously constrain both the stellar compactness and the hot spot and viewing geometries. Thus future large area timing experiments, such as the proposed Timing of Extreme X-ray Astrophysical Sources (TEXAS) experiment, will be extremely powerful tools for probing the structure of neutron stars.

We thank Cole Miller, Craig Markwardt and Tim Olson for many helpful discussions and comments on the manuscript. We thank Cole Miller for providing some of the mass - radius relations for the equations of state shown in Figure 6. We also thank Tim Olson for providing the mass radius relations based on kinetic theory constraints to the APR equation of state.

## REFERENCES

Akmal, A., Pandharipande, V. R. & Ravenhall, D. G. 1998, Phys. Rev. C, 58, 1804

Chandrasekhar, S. 1960, Radiative Transfer (New York: Dover)

Chen, K. & Shaham, J. 1989, ApJ, 339, 279

Heise, J. et al. 2000, Talk presented at AAS HEAD meeting, Honolulu, HI

Heiselberg, H. & Hjorth-Jensen, M. 1999, ApJ, 525, L45

Joss, P. C. 1978, ApJ, 225, L123

Lattimer, J. M. & Prakash, M. 2000, ApJ, in press, (astro-ph/0002232)

London, R. A., Taam, R. E. & Howard, W. M. 1986, ApJ, 306, 170

Miller, M. C. & Lamb, F. K. 1996, ApJ, 470, 1033

Miller, M.C. & Lamb, F.K. 1998, ApJ, 499, L37

Miller, M.C. 1999, ApJ, 515, L77

Miller, M. C., Lamb, F. K. & Psaltis, D. 1998, ApJ, 508, 791

Mendez, M., van der Klis, M. & van Paradijs, J. 1998, ApJ, 506, L117

Olson, T. S. 2001, Phys. Rev. C, 63, 015802

Pandharipande, V. R., & Smith, R. A. 1975, Phys. Lett., 59B, 15

Pechenick, K. R., Ftaclas, C. & Cohen, J. M. 1983, ApJ, 274, 846

Psaltis, D. Ozel, F. & DeDeo, S. 2001, ApJ, in press, (astro-ph/0004387)

Strohmayer, T. E. 2001, Advances Sp. Res. submitted, (astro-ph/0012516)

Strohmayer, T. E., Zhang, W., Swank, J. H., White, N. E. & Lapidus, I. 1998a, *ApJ*, 498, L135

Strohmayer, T. E., Jahoda, K., Giles, A. B. & Lee, U. 1997, *ApJ*, 486, 355

Strohmayer, T. E., Zhang, W., & Swank, J. H. 1997, *ApJ*, 487, L77

Strohmayer, T. E., Zhang, W., Swank, J. H., Smale, A. P., Titarchuk, L., Day, C. & Lee, U. 1996, *ApJ*, 469, L9

Strohmayer, T. E. 1992, *ApJ*, 388, 138

Thorsett, S. E. & Chakrabarty, D. 1999, *ApJ*, 512, 288

Weinberg, N., Miller, M. C. & Lamb, D. Q. 2000, *ApJ*, submitted, (astro-ph/0001544)

## 6. Figure Captions

Fig. 1.— Geometry for calculation of the flux from a hot spot on a rotating neutron star. Here the hot spot is situated on the rotational equator. See the text for a description of the relationship between the angles  $\phi$ ,  $\psi$  and the impact parameter,  $b$ .

Fig. 2.— Light-curves generated with the rotating hot spot model for different values of the neutron star compactness. Notice the decrease in amplitude with increasing compactness. Note also the decrease in amplitude and increase in flux as the hot spot spreads to encompass the entire surface. These models were computed with one hot spot assuming isotropic emission from the surface. The top three curves have been displaced vertically for clarity. The qualitative behavior of the amplitude with compactness,  $M/R$ , using the grey atmosphere beaming function is the same, only the modulation amplitudes differ slightly.

Fig. 3.— Model fits to the bursts from 4U 1636-53. Each panel shows the data (histogram) and model (thick solid curve) fit to the rising portion of a burst. The dashed vertical lines denote the time interval in which we fit the hot spot model. The extent of each model curve covers the total time it takes for the hot spots to envelope the entire neutron star surface. The bursts are labelled by date.

Fig. 4.— Data and best fit models for several fits to the December 28th, 1996 burst from 4U 1636-53. Shown are fits using two hot spots with  $\theta_s = \theta_{obs} = 0$  (solid); one hot spot with  $M/R$  fixed at 0.284 and  $\theta_s = \theta_{obs} = 0$  (dashed); and one hot spot with  $\theta_s$  and  $\theta_{obs}$  free to vary (dotted). All the fits shown were computed with the grey atmosphere beaming function.

Fig. 5.— Compactness constraints for the four bursts from 4U 1636-53. The solid horizontal line is the best fitting constant value of compactness,  $\beta_{avg}$ . The dashed and dot-dashed lines

are the 90 and 99% confidence upper limits on  $\beta_{avg}$ . The burst number corresponds to their position in Table 1.

Fig. 6.— Summary of mass radius constraints from fits to bursts from 4U 1636-53 using the two spot model and the grey atmosphere beaming function. The diagonal dashed lines show the 90 and 99 % confidence upper limits for  $M/R$  from the four fits in Table 1 (see also Figure 5). The shaded region is the allowed range of  $M$  and  $R$  which satisfies the compactness constraints and has  $M > 1.4M_{\odot}$ . The solid diagonal line corresponds to our computational limit,  $M/R = 0.284$ . The other curves show mass - radius relations for equations of state FPS (Lorenz et al. 1993), L (Pandharipande & Smith 1975b), and APR (Akmal, Pandharipande & Ravenhall 1998), which range from very soft (FPS) to very stiff (L). We also show two different modifications to the APR EOS based on the relativistic kinetic theory constraints of Olson (2001) (thick dashed curves). The two curves correspond to the use of different matching densities for the high density kinetic theory constraints (see §5 and Olson 2001). The results favor stiffer equations of state with  $R > 11.5$  km for a  $1.4 M_{\odot}$  neutron star.

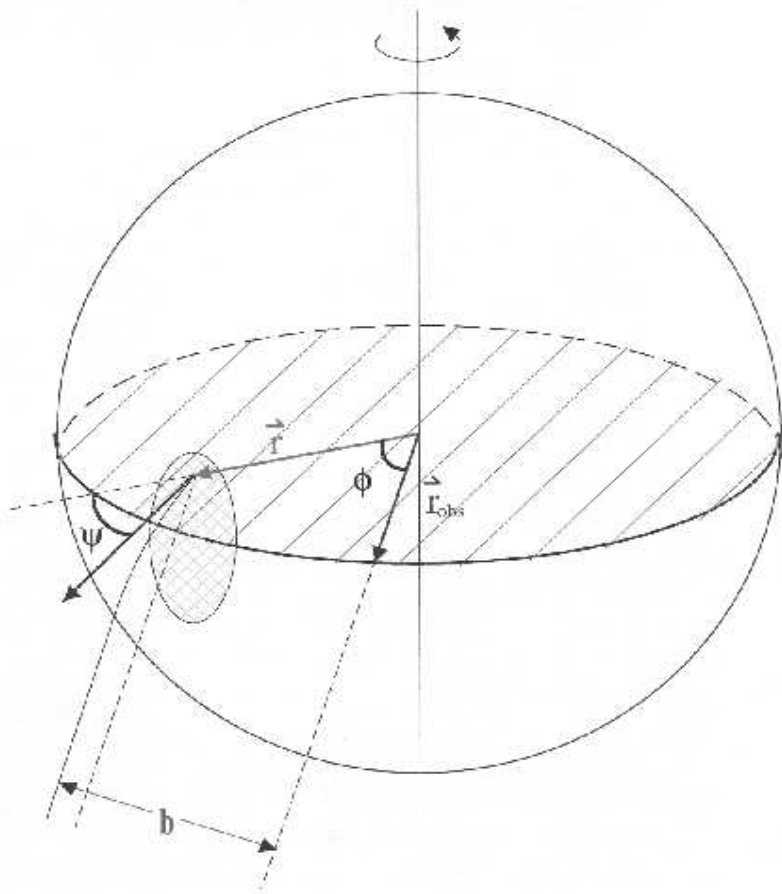


Figure 1: Geometry for calculation of the flux from a hot spot on a rotating neutron star.

Here the hot spot is situated on the rotational equator. See the text for a description of the relationship between the angles  $\phi$ ,  $\psi$  and the impact parameter,  $b$ .

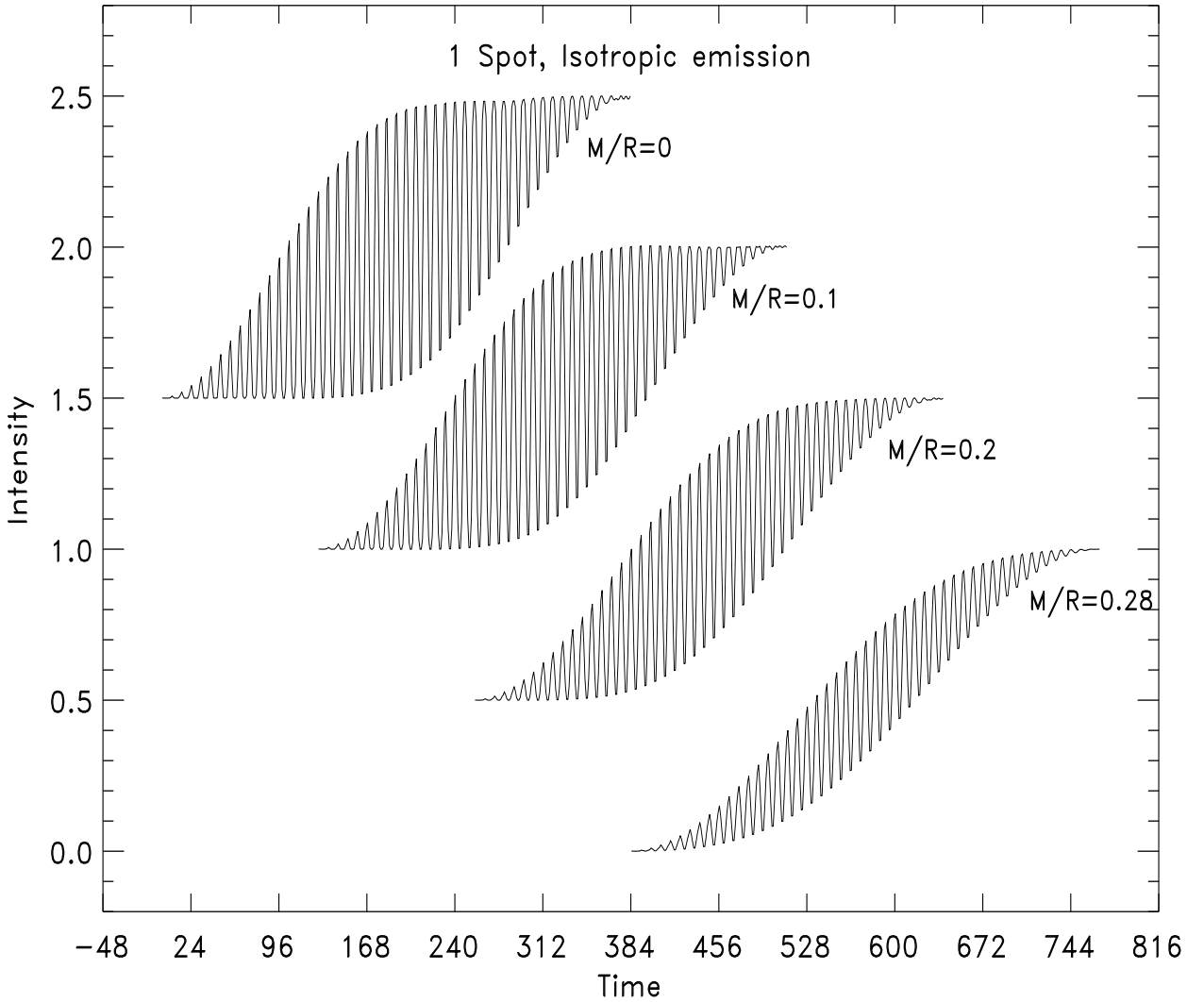


Figure 2: Light-curves generated with the rotating hot spot model for different values of the neutron star compactness. Notice the decrease in amplitude with increasing compactness. Note also the decrease in amplitude and increase in flux as the hot spot spreads to encompass the entire surface. These models were computed with one hot spot assuming isotropic emission from the surface. The top three curves have been displaced vertically for clarity. The curves were computed using isotropic emission from the surface, the qualitative behavior of the amplitude with compactness,  $M/R$ , using the grey atmosphere beaming function is the same, only the modulation amplitudes differ slightly.

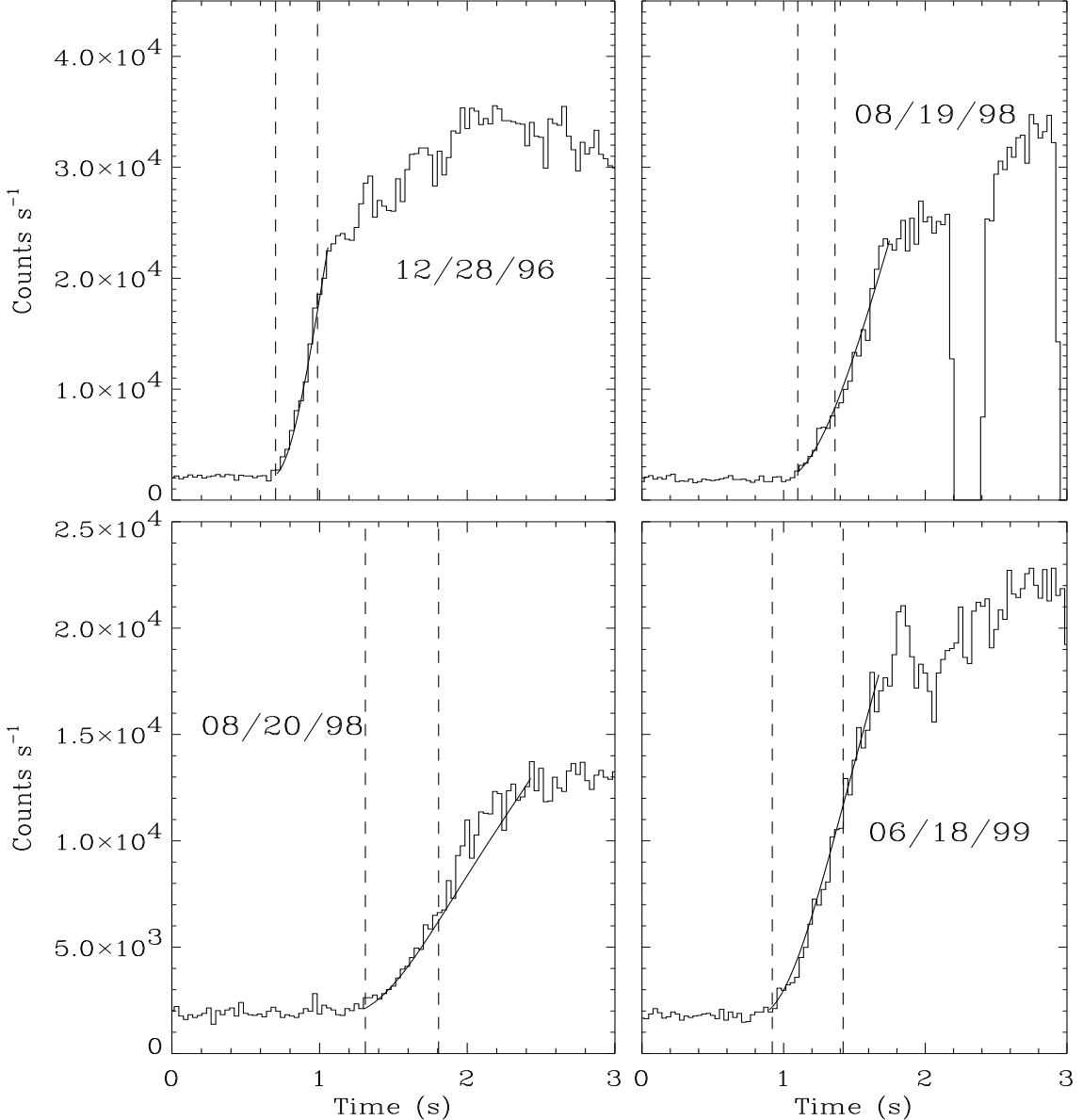


Figure 3: Model fits to the bursts from 4U 1636-53. Each panel shows the data (histogram) and model (thick solid curve) fit to the rising portion of a burst. The dashed vertical lines denote the time interval in which we fit the hot spot model. The extent of each model curve covers the total time it takes for the hot spots to envelope the entire neutron star surface. The bursts are labelled by date.

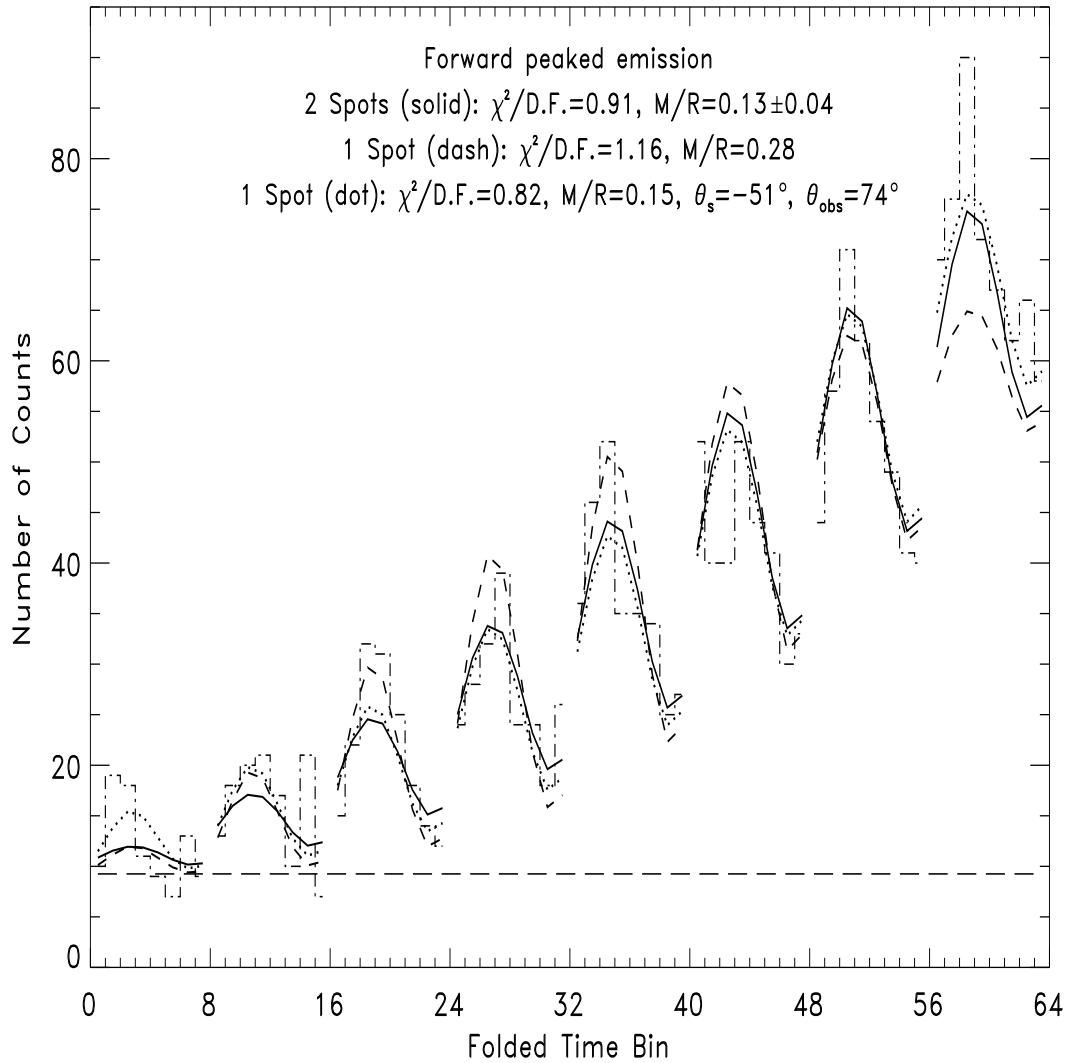


Figure 4: Data and best fit models for several fits to the December 28th, 1996 burst from 4U 1636-53. Shown are fits using two hot spots with  $\theta_s = \theta_{\text{obs}} = 0$  (solid); one hot spot with  $M/R$  fixed at 0.284 and  $\theta_s = \theta_{\text{obs}} = 0$  (dashed); and one hot spot with  $\theta_s$  and  $\theta_{\text{obs}}$  free to vary (dotted). All the fits shown were computed with the grey atmosphere beaming function.

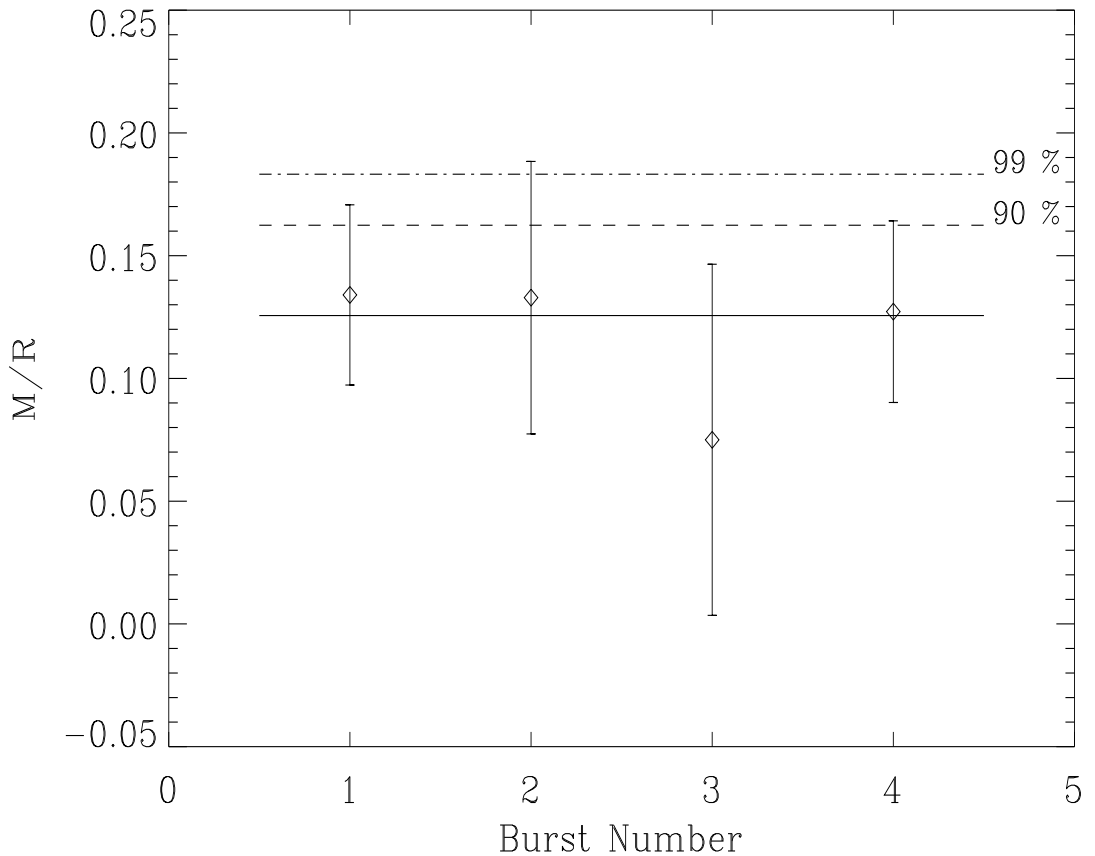


Figure 5: Compactness constraints for the four bursts from 4U 1636-53. The solid horizontal line is the best fitting constant value of compactness,  $\beta_{avg}$ . The dashed and dot-dashed lines are the 90 and 99% confidence upper limits on  $\beta_{avg}$ . The burst number corresponds to their position in Table 1.

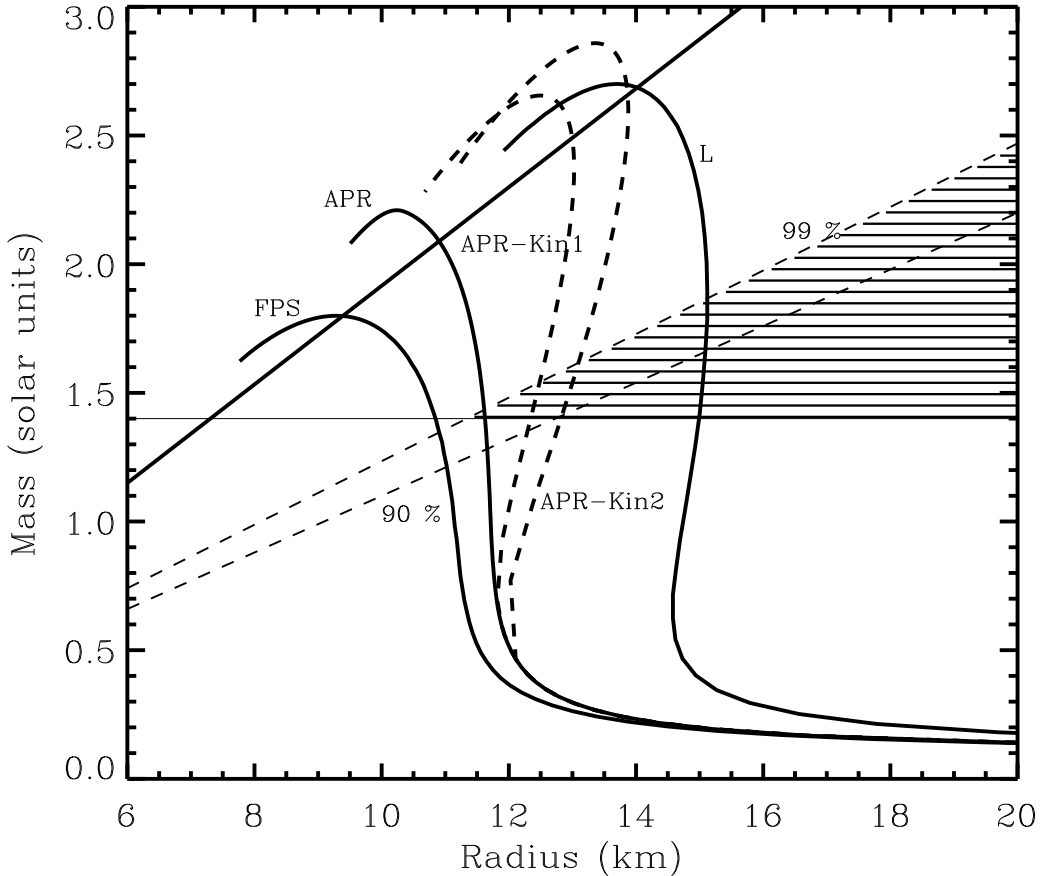


Figure 6: Summary of mass radius constraints from fits to bursts from 4U 1636-53 using the two spot model and the grey atmosphere beaming function. The diagonal dashed lines show the 90 and 99 % confidence upper limits for  $M/R$  from the four fits in Table 1 (see also Figure 5). The shaded region is the allowed range of  $M$  and  $R$  which satisfies the compactness constraints and has  $M > 1.4M_{\odot}$ . The solid diagonal line corresponds to our computational limit,  $M/R = 0.284$ . The other curves show mass - radius relations for equations of state FPS (Lorenz et al. 1993), L (Pandharipande & Smith 1975b), and APR (Akmal, Pandharipande & Ravenhall 1998), which range from very soft (FPS) to very stiff (L). We also show two different modifications to the APR EOS based on the relativistic kinetic theory constraints of Olson (2001) (thick dashed curves). The two curves correspond to the use of different matching densities for the high density kinetic theory constraints (see §5 and Olson 2001). The results favor stiffer equations of state with  $R > 11.5$  km for a  $1.4 M_{\odot}$  neutron star.

Table 1. Summary of Fits to Burst Oscillations in 4U1636-53 and 4U 1728-34<sup>a</sup>

Epoch (UTC)	$\Delta T_{fit}$ (s)	$\beta = M/R$	$S$ (cts $s^{-1}$ ster $^{-1}$ ) <sup>c</sup>	$\alpha_0$ (deg)	$\dot{\alpha}$ (deg $s^{-1}$ )	$\delta_0$ <sup>b</sup>	$\chi^2$
4U 1636-53							
12/28/96 at 22:39:34	0.276	$0.134 \pm 0.037$	1641.6	$6.41 \pm 1.6$	$222.9 \pm 39.6$	116.7	53.6
08/19/98 at 11:47:07	0.303	$0.133 \pm 0.056$	1716.1	$14.38 \pm 3.8$	$130.7 \pm 54.3$	81.0	63.7
08/20/98 at 05:16:35	0.496	$0.075 \pm 0.072$	882.1	$8.66 \pm 3.0$	$69.5 \pm 36.0$	-3.0	65.3
06/18/99 at 23:50:10	0.460	$0.127 \pm 0.037$	1272.3	$6.70 \pm 1.4$	$102.4 \pm 22.2$	14.8	61.5
4U 1728-34							
02/16/96 at 10:00:49	0.221	$0.113 \pm 0.042$	1238.7	$9.1 \pm 2.2$	$370.8 \pm 39.6$	102.7	69.7
09/21/97 at 18:10:56	0.354	$0.130 \pm 0.043$	1001.9	$7.4 \pm 2.0$	$181.8 \pm 32.4$	142.1	54.6

<sup>a</sup>All fits are for two hot spots assuming the grey atmosphere beaming function, and have 59 degrees of freedom.

<sup>b</sup>The initial phase is an azimuthal angle, measured with respect to the observers direction, and counted positive in the anti-clockwise rotational direction of the neutron star. It can be determined to  $\lesssim 1\%$ .

<sup>c</sup>The normalization  $S$  is given in terms of the counting rate per unit solid angle of the neutron star covered by the hot spot(s). For example, the peak counting rate can be determined for a given burst by multiplying  $S$  by  $4\pi$ . The uncertainty in  $S$  is typically about 30%. This results from the fact that  $S$  is strongly correlated with both  $\dot{\alpha}$  and  $\beta$ .